Hierarchical Control of Distributed Battery Energy Storage System in a DC Microgrid

Jing Zhang
Department of Systems Engineering
Universitry of Arkansas at Little Rock
Little Rock, AR. USA
jxzhang1@ualr.edu

Jeffrey T. Csank
Power Systems Branch
NASA Glenn Research Center
Cleveland, OH. USA
jeffrey.t.csank@nasa.gov

James F. Soeder
Power Systems Branch
NASA Glenn Research Center
Cleveland, OH. USA
james.f.soeder@nasa.gov

***Abstract*— This paper presents a novel hierarchical control approach of a DC microgrid (DCMG) which is supplied by a distributed battery energy storage system (BESS). With this approach, all battery units distributed in the BESS can be controlled to discharge with accurate current sharing and state-of-charge (SoC) balancing. Similar to other hierarchical control approaches used in DCMGs, this approach consists of three levels: (1) primary control, (2) secondary control and (3) tertiary control. This work includes defining a unit control error (UCE) at the secondary control level and evaluating current sharing weights at tertiary control level. A centralized controller at secondary control level is designed to detect the UCEs of each battery unit, and to restore the average voltage of a DCMG and control battery current sharing simultaneously. The distributed battery units share the load current in a DCMG based on weights. These weights are evaluated at the tertiary control level based on battery SoCs. The approach's effectiveness was confirmed in digital simulation tests with the same simulation model as used in the NASA AMPS Modular Hardware Emulator.**

Keywords*— NASA, Gateway, DC microgrid, hierarchical control, battery, power, energy

NOMENCLATURE

B_I	= coefficient of current sharing error
I_{Oi}	= output current of i-th battery charge/discharge unit
K_C	= gain of secondary controller
K_{DP}	= Slope of droop control
K_w	= gain of SoC controller
P_L	= power of a load
R_{DP}	= virtual resistance of droop control
r_{Oi}	= output resistance of a battery charge/discharge unit
r_L	= resistance of a distribution line
SoC	= state-of-charge of a battery
T_s	= sample and control period of a discrete-time controller
UCE_i	= unit control error of i-th battery charge/discharge unit
V_{Oi}	= output voltage of i-th battery charge/discharge unit
V_{set}	= setting voltage
w_i	= weights of load power sharing

I. INTRODUCTION

DC microgrids (DCMG) are becoming more widely used today in aerospace and terrestrial applications to supply highly reliable power and/or power produced from clean energy. In many of these applications, such as the International Space Station (ISS) [3,4], batteries are the only available energy sources at certain times to supply power to the loads. In a DCMG, a battery energy storage system (BESS) with multiple battery units (BUs) may be in a centralized or distributed architecture [5,6]. In this work, a battery unit (BU) is reference to a battery with its battery charge/discharge units (BCDU). In a centralized BESS, all BUs are installed together at one location. It is convenient to manage the operation and control load sharing of all BUs. In a distributed BESS, the BUs are scattered throughout the DCMG. This design may substantially improve the system flexibility and reliability for modular-based DCMGs. However, one of the challenges for a distributed BESS is to keep the load sharing accuracy and battery state-of-charge (SoC) balanced among the BUs distributed in a DCMG.

Although a centralized BESS was adopted for the ISS electrical power system (EPS) [3], a distributed BESS application is of interest to NASA for the Gateway electrical power system. The Gateway will be an outpost orbiting the Moon that provides vital support for a sustainable [2]. long-term human return to the lunar surface, as well as a staging point for deep space exploration [7-9]. The initial phase of the Gateway consists of two modules, a Power and Propulsion Element (PPE) and Habitational and Logistics Outpost (HALO) module.

The Gateway reference system consists of two independent power channels across two modules. Each channel in one module is equipped with one BU of the same capacity. Each power channel is supplied by one solar power generation unit (centralized power supply) during insolation time. During an eclipse, the entire system is supplied with the distributed BUs. In this application where power flow is designed to be unidirectional, without proper regulation a battery upstream can be discharged to its limit too quickly and force all power to be delivered from the remaining BUs. This situation can be escalated by other power system failures that remove power sharing from other devices and can result in a blackout of loads. Hence, it is significant to develop an approach to implement uniform discharge of all batteries so that the system can keep the maximum power capacity until all batteries are fully discharged [33]. Figure 1 shows one power channel of the Gateway EPS with two distributed BUs. In this work, it is treated as a DCMG with a distributed BESS.

Hierarchical control is a standard control strategy in traditional AC power systems [1]. This approach includes three control levels: (1) primary control, (2) secondary control and (3)

tertiary control. Primary control, or droop control, is used to control a generator power output based on the line frequency in a droop characteristic. With the droop control strategy, all generators in a power system can automatically share the loads based on their power ratings and power setting. The secondary control level is also referred to as load-frequency control. The basic objectives of the secondary control for an interconnected area are to restore the line frequency and maintain the net tie-line power flow at its scheduled value. The area control error includes frequency error and net tie-line power flow error. The third level, tertiary control, includes all other system level control strategies including system operation and optimal power flow control. Each of these three-control levels operate at different timescales [32]. The operational timescale of primary control is up to 10 seconds, while it takes minutes for secondary control to recover the line frequency to its nominal value. Tertiary control operates at a much slower timescale ranging from about 15 minutes to several hours.

The hierarchical control strategy has been widely applied to DCMG research works [10-31]. In the reported applications, droop control is adopted at the primary control level. Different from the droop control in AC power grids, the droop control of DCMGs is mainly based on the measured bus voltages or output currents of DC source converters, which results in significant errors of load current or power sharing among the DC source converters in the DCMG and DC bus voltage deviation. In many published papers on DCMGs [21-31], the objectives of secondary control are to restore the DC bus voltage deviation caused by primary droop control and enhance the load current sharing accuracy. The tertiary control in DCMGs implements additional system control and operation strategies, such as balancing SoC control of distributed battery energy storages.

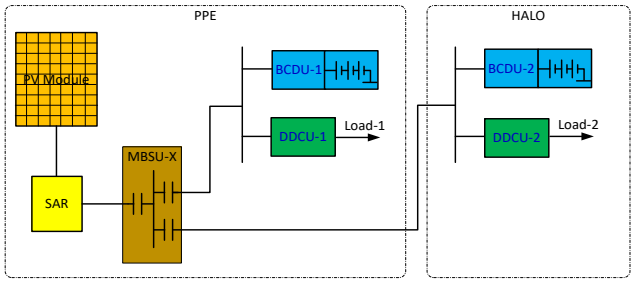

Fig 1. Distributed BESS with two BUs Designed for the Gateway EPS

To enhance the load current/power sharing accuracy, there are a number of strategies reported for secondary control. A simple solution is to set a large droop gain with a voltage shifting at the secondary control level [26]. The droop gain should be set so large that the cable resistances can be neglected compared to the virtual resistance of the droop control. Another important strategy presented in published literature is to design an adaptive controller of droop gain at secondary control [27, 29]. This control approach will automatically adjust the droop gain used at the primary control level. To enhance the bus voltage control and load current/power sharing accuracy simultaneously, secondary control for each DC source converter can also be implemented based on an average voltage controller and an average current/power controller [21, 28]. To obtain average voltage and average current/power, network communication in a DCMG is necessary. Such a secondary control strategy will be implemented in a microgrid central controller (MGCC).

Inspired by the hierarchical control used in traditional AC power grids, a hierarchical control approach for a DCMG with a distributed BESS is proposed in this work. Like many reported DCMGs, droop control is adopted as the primary control strategy and implemented in each BU. At secondary control level, a unit control error (UCE) is defined for each BU in the system. The UCE includes the deviation of average voltage from desired voltage and current sharing error of each BU. The controller at the secondary control level adjusts the BCDU setting voltage for each BU so that its UCE reaches zero in steady state. Finally, the strategy of tertiary control is to adjust the weights of load sharing of each DC source converter based on each battery state-of-charge (SoC).

The remainder of this paper is organized into the following sections: (1) BU current sharing with droop control, (2) hierarchical control approach, (3) secondary control, (4) tertiary control, (5) simulation test results, and (6) conclusions.

II. BU Current Sharing with Droop Control

Droop control is generally adopted at the primary control level. Droop control is effective to implement accurate current sharing among BUs in a centralized BESS where cable resistances from all BUs to a shared bus can be kept almost equal. However, in a distributed BESS, it is difficult to keep equal cable resistances from BUs to loads. It will result in a significant error in current sharing if only droop control is used [2]. To evaluate the battery current sharing error, power flow analysis is performed for the distributed BESS with two BUs designed for the Gateway EPS as shown in Figure 1. During eclipse, solar power is not available. The EPS is only supplied by two BUs. BCDU-1 and BCDU-2 control the batteries' current sharing in droop control. Loads in the PPE and HALO modules are powered by two DC/DC converter units (DDCU-1 and DDCU-2). These are treated as constant power loads (CPLs).

In droop control, a BCDU will control the output current based on the BCDU setting voltage and its output voltage in (1),

$$I_O = K_{DP}(V_{set} - V_O) \tag{1}$$

The droop characteristic is shown in Fig. 2(b). A battery and its BCDU with droop control can be represented with a Thevenin equivalent circuit as shown in Fig. 2(c). R_{DP} is a virtual resistor, or a droop gain [10]. Its value is the reciprocal of the slope K_{DP}: $R_{DP} = 1/K_{DP}$. This equivalent circuit is useful for the following power flow analysis.

Power flow analysis is a numerical method widely used in conventional AC power systems. It is effective to find all four fundamental parameters at each bus in steady state by solving nonlinear equations in voltage magnitudes, phase shifts, real power and reactive power of all busses in a power grid. Compared with a bus in an AC power grid, a bus in a DCMG has only two fundamental parameters: voltage and power. In the system shown in Fig. 1, there is no physical bus available which can be treated as a slack bus or voltage controlled bus.

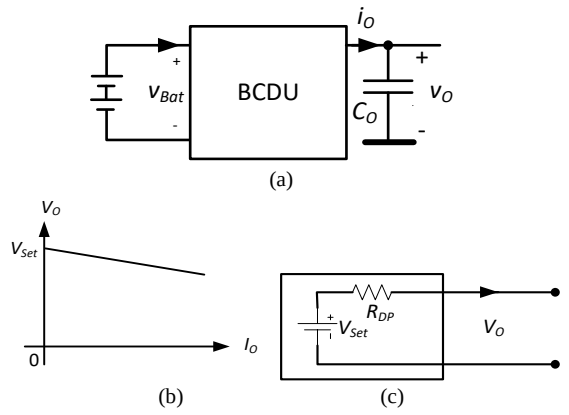

Fig 2. (a) a battery unit, (b) droop characteristics, (c) equivalent circuit

Therefore, the typical method must be modified so that it may be used in this work. The one line diagram of the subsystem is shown in Fig. 3. Bus #1 to #8 are named for use in the power flow analysis. Each BCDU is represented as an ideal voltage source and a virtual resistor, i.e. V_{set1} and R_{13} for BCDU-1, V_{set2} and R_{24} for BCDU-2. Bus #1 and #2 are virtual voltage-controlled buses with the fixed bus voltages V_{set1} and V_{set2}, respectively. The virtual resistances R_{13} and R_{24} are equal to $R_{DP} = 1/K_{DP}$. R_{35} is the line resistance from BCDU-1 output to the main bus switching unit MBSU-1, and R_{46} the line resistance from BCDU-2 output to MBSU-2. R_{56} is the total line resistance from MBSU-1 to MBSU-2. R_{57} is the line resistance between DDCU-1 output and MBSU-1. R_{68} is the line resistance between DDCU-2 output and MBSU-2. Bus #3 and #4 are the outputs of two BCDUs, and bus #5 and #6 are MBSU-1 and MBSU-2. Bus #7 and #8 are the inputs of DDCU-1 and DDCU-2. All resistances are listed in Table 1.

$$P_i = \sum_{k=1}^{8} Y_{ik} V_i V_k \quad \text{for } i = 1, 2, \dots, 8 \qquad (2)$$

where P_i is the power injected into the i-th bus. The coefficients Y_{ik} are the elements of the admittance matrix of the network in Fig. 3. The given conditions are: $V_1 = V_{set1}$, $V_2 = V_{set2}$, $P_i = 0$ for $i = 3, 4, 5, 6$, $P_7 = -P_{L1}$, $P_8 = -P_{L2}$.

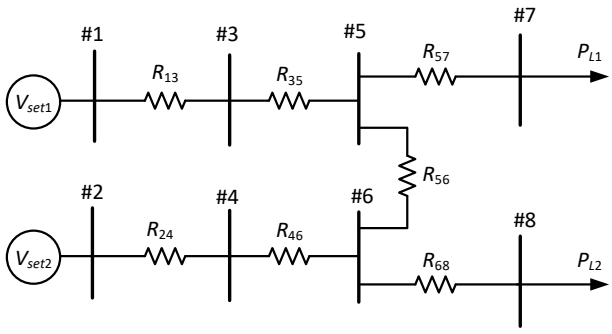

Fig 3. System one-line diagram for power flow analysis

TABLE I. RESISTANCES IN ONE-LINE DIAGRAM OF FIG. 3

R_{13} (Ω)	R_{24} (Ω)	R_{35} (Ω)	R_{46} (Ω)	R_{57} (Ω)	R_{68} (Ω)	R_{56} (Ω)
0.019	0.019	0.025	0.025	0.005	0.005	0.06

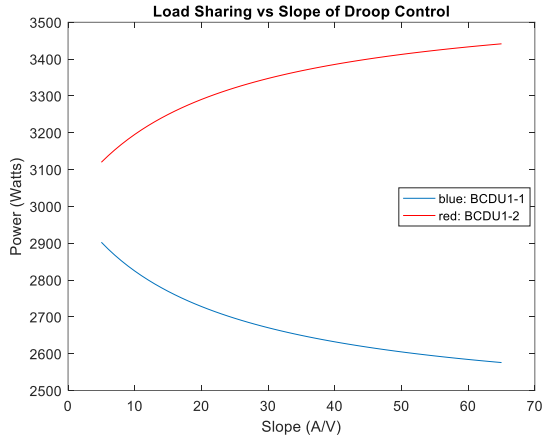

Fig 4. (a) Current sharing vs droop slope, (b) BCDU output voltages vs droop slope

A MATLAB program based on the Newton-Raphson method was developed to find the numerical solutions of (2) at the load power settings: P_{L1} = 1864.67 W, P_{L2} = 4111.36 W. The computation was done for different slopes of droop control from 5 A/V to 65 A/V. The computational results of the output power and voltages of the two BCDUs as functions of the slope are shown in Fig. 4(a) and (b). When the droop slope decreases, the virtual resistances increase compared to the other resistances in Fig. 3. It will improve the power sharing between two BUs passively as shown in Fig. 4(a). However, an increase of the virtual resistance will significantly increase the voltage drop at each BCDU output as shown in Fig. 4(b) and will result in a power quality problem. The results of the power flow analysis show that the droop control alone cannot implement accurate current sharing in a distributed BESS. The current sharing effect of the droop control is controlled by the virtual resistances introduced into the circuit. Compared with the

resistances of the system under the rated conditions as listed in Table 1, the cable resistances are larger than the virtual resistances, resulting in this style of droop control being ineffective for current sharing between two BUs. Generally, BU current sharing by droop control will significantly degrade in the case of a low voltage but large current DCMG with a distributed BESS.

III. Hierarchical Control Approach

To enhance BU current sharing during a discharging operation, a hierarchical control approach for the distributed BESS is developed and evaluated in this work. The control architecture is shown in Fig. 5. It includes three control levels: primary control (bottom level), secondary control and tertiary control (top level).

The primary control is the droop control implemented in the BCDU of each BU. The objectives of the primary control are: (1) to ensure a stable system operation; and (2) to control local bus voltage and implement passive load current/power sharing. In the proposed approach, it is assumed that the droop control of all BCDUs in the system have the same slope $K_{DP} = 52$ A/V.

The secondary control is an approach developed in this work. The objectives of the secondary control layer are (1) to restore then average output voltages of the DCMG back to the setting value of 120 V; and (2) to enhance accurate current sharing of all distributed BUs according to desired sharing weights.

With the proposed primary control and secondary control, the restoration of the average output voltage of all BCDUs and accurate current sharing among the BUs in the system can be implemented simultaneously. The primary control is distributed in each BCDU. The bandwidth of the primary control loop can be above 100 Hz. The secondary control is discrete and implemented in the MGCC. It will collect sensed voltage and current values from all BUs, generate voltage setting commands and update the commands of all BCDUs through a communication network. On the existing simulation test platform, the AMPS Modular Hardware Emulator, the secondary controller completes these operations once every second.

The objective of the tertiary control is to implement additional control functions related to battery energy management and other special events so that the system can stay in an optimal configuration. A typical function is the control of battery SoCs, in which all battery SoCs are kept equal during a discharging operation when all BUs begin with the same initial SoC value. This ensures the maximum power capability of the distributed BESS before all batteries are fully discharged. If there is a significant difference between initial battery SoCs, the tertiary control will be able to schedule the weight for each BU so that all battery SoCs can equalize as soon as possible.

Like the secondary control, the proposed tertiary control is discrete time and implemented in the MGCC. Additional control functions can be developed for handling other special events. For example, if one battery is out of order, the tertiary control should be able to adjust the weight scheduling function. The tertiary controller will be able to switch from one control function to another based on different operation states.

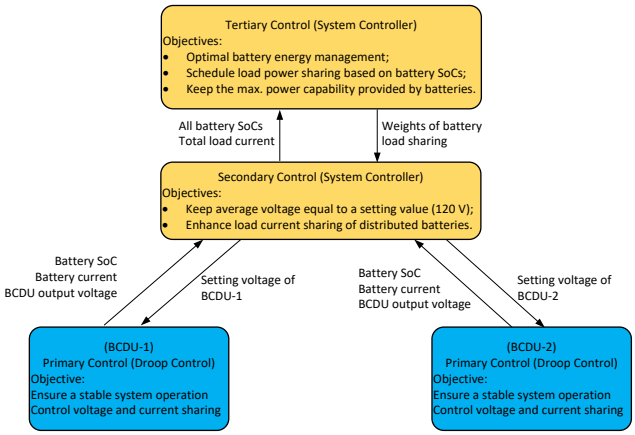

Fig. 5.Three-level hierarchical control

IV. Unit Control Error and Secondary Control Implementation

As aforementioned, secondary control is designed to control the average BCDU output voltage and enhance the accurate current sharing between distributed BUs. The proposed approach of secondary control is explained in the following sections.

A. *Definition of Unit Control Error*

Fig. 6 presents the block diagram of secondary control of a distributed BESS with two BUs. The secondary controller is shown in the orange block. Through a communication network, the secondary controller will sample output voltages and currents, and calculate unit control errors (UCE) of two BCDUs. UCEs of two BCDUs are defined in the following formulae,

$$UCE_1 = \frac{V_{O1} + V_{O2}}{2} - V_{set} + B_I[I_{O1} - w_1(I_{O1} + I_{O2})] \quad (3a)$$

$$UCE_2 = \frac{V_{O1} + V_{O2}}{2} - V_{set} + B_I[I_{O2} - w_2(I_{O1} + I_{O2})] \quad (3b)$$

where V_{O1} and V_{O2} are the output voltages of BCDU-1 and BCDU-2, and I_{O1} and I_{O2} the output currents. The sum of the two battery currents $I_{O1} + I_{O2}$ is the total load current of the distributed BESS. V_{set} is the desired DCMG working voltage. w_1 and w_2 are the weights of current sharing of each respective BUwhere $w_1 + w_2 = 1$, and $w_1 \geq 0, w_2 \geq 0$. B_I is the coefficient of current sharing error.

An integral controller is used to accumulate the UCE of each BU and generate the voltage setting for the respective BCDU. Because of the integral controller, the UCEs of the two BUs will reach zero in steady state if the system is stable. In this state, Eq. (3a, b) yields,

$$\frac{V_{O1}+V_{O2}}{2}=V_{set}$$

$$I_{O1}=w_1(I_{O1}+I_{O2}),\quad I_{O2}=w_2(I_{O1}+I_{O2})$$

The results show that the average output voltage of BCDUs is equal to the desired setting voltage and the output currents are equal to the desired current sharing.

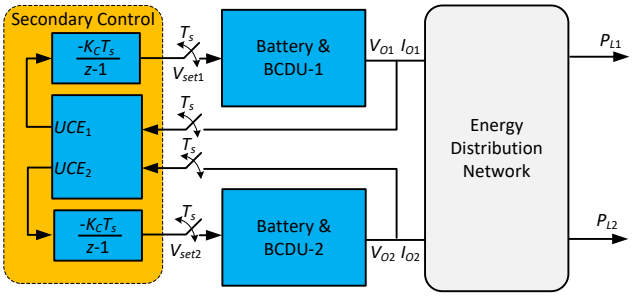

Fig. 6. Block diagram of secondary control of two-BESS subsystem

Although the discussion above is for a distributed BESS with two BUs, the method is easily extended to a general system with *N* BUs. In such a system, the unit control error for each BCDU is,

$$UCE_i=\frac{1}{N}\sum_{k=1}^{N}V_{Ok}-V_{set}+B_I\left(I_{Oi}-w_i\sum_{k=1}^{N}I_{Ok}\right)$$

$$\text{for } i=1,2,\dots\dots,N \tag{4}$$

where $\sum_{i=1}^{N}w_i=1$, and $w_i\geq 0$ for $i=1,2,\dots\dots,N$.

B. *Coefficient B_I and Gain K_C*

The coefficient B_I is a current bias constant which affects the required change of a BCDU setting voltage to compensate the current sharing error of the BCDU. The value is related to the resistances in the network which affect the power sharing between BUs.

The controller used in the secondary control is a discrete-time integral control with the gain K_C and sampling period T_s. This controller implements the control of two quantities in a distributed BESS: (1) average output voltages of the BCDUs and (2) current sharing of each BU. The selection of the gain is restricted by the system stability of the voltage control and current sharing control.

Compared to the dynamic behavior of the primary control of the distributed BESS, the sampling period of the secondary control is generally quite large, for example 1 second. We can assume that the distributed BESS is stable under the primary control and can reach its steady state within one sampling period after its setting is updated at the beginning of the sampling period. The restriction of the control gain K_C for a stable secondary control loop is

$$K_CT_s<\min\left(1,\frac{R_{13}+R_{24}+R_{35}+R_{46}+R_{56}}{2B_I}\right) \tag{5}$$

The gain K_C is related to the sampling/control period T_s and the coefficient B_I. For $T_s=1$ second, the gain must be set less than 1.

If $B_I<\frac{2R_{DP}+r_{O1}+r_{O2}+r_{Line}}{2}$, or the coefficient B_I is small enough compared to the sum of the resistances, it will not affect the system stability, and hence, $K_CT_s<1$. Otherwise, $K_CT_s<\frac{2R_{DP}+r_{O1}+r_{O2}+r_{Line}}{2B_I}$.

In the simulation tests, we take the resistances listed in Table 1. The gain limit vs the coefficient B_I is shown in Fig. 7.

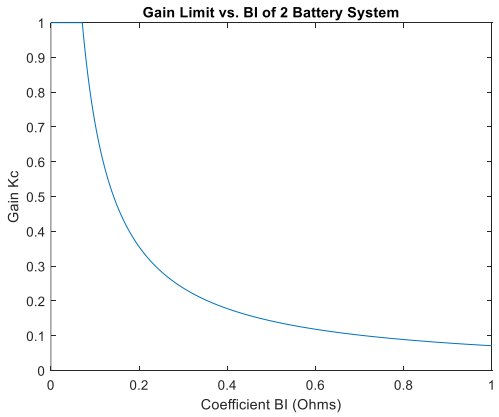

Fig. 7. Restriction of gain KC of the distributed BESS

V. Tertiary Control

Tertiary control is designed to schedule the weights of current sharing. The exact objective of the control can be different depending on the system operating state. For example, one might regulate current sharing based on battery SoCs, or optimize current sharing for a special event. Different objectives will result in different approaches used in the tertiary control. The approach to implement SoC balancing control is discussed here.

One objective for the current sharing strategy is to keep the SoCs of all batteries equal during discharging. The advantage of this objective is the ability to ensure the maximum power capability of the system until all batteries are fully discharged. For example, consider a system where each BU has the maximum rated power of 5 kW. For a BESS with two BUs, the maximum power capability is 10 kW. If one battery is fully discharged before another, the maximum power capability is reduced to only 5 kW.

The strategy of tertiary control is designed as shown in Figure 8. The weights generated in the first block of the tertiary controller are,

$$\begin{cases}w_1=0.5+\Delta w_1\\ w_2=0.5+\Delta w_2\end{cases} \tag{6}$$

where, Δw_1 and Δw_2 are calculated as

$$\Delta w_1 = K_w\left(SoC_1 - SoC_{sys}\right)$$

$$\Delta w_2 = K_w\left(SoC_2 - SoC_{sys}\right)$$

And they are limited within the range (-0.5, 0.5).

$SoC_{sys} = \frac{1}{2}\sum_{k=1}^{2} SoC_k$ is referred to as BESS state of charge.

The second block will generate weight settings ($w_{1,set}$, $w_{2,set}$) by evaluating the weights (w_1, w_2) based on the total current requirement $I_{Bat,tot}$ and the maximum BU current $I_{Bat,max}$ so that the weight settings will not result in over-current. Fig. 9 shows the flow chart of the function in the second block of Fig. 8.

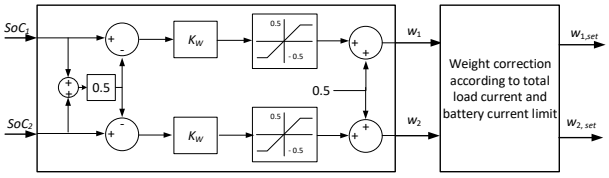

Fig. 8. Block diagram of tertiary control

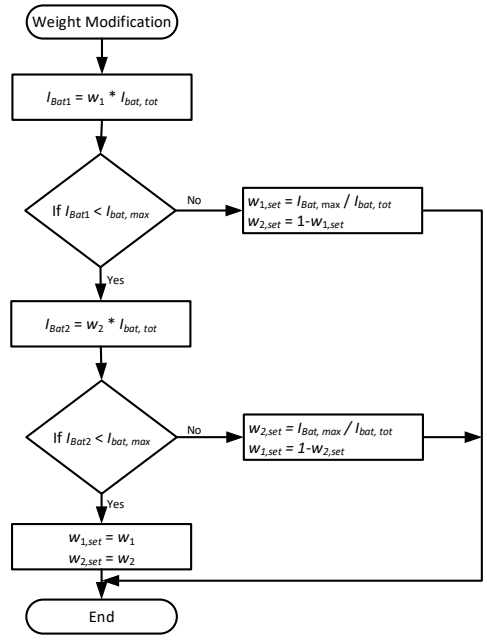

Fig. 9. Flow chart for weight modification in tertiary control

VI. Simulation Test Results

Up to now, the proposed secondary control and tertiary control have been tested with a simulation model in SIMULINK, of which all parameters and important features matched those in the NASA AMPS Modular Hardware Emulator. The effectiveness of the secondary control has also been confirmed on the NASA test platform AMPS Modular Hardware Emulator.[7] Some important simulation test results with the SIMULINK model are now presented. In all following figures of the simulation tests, the quantities of BCDU-1 are shown in red dash-dotted lines and the quantities of BCDU-2 in blue lines.

Figures 10 to 13 are the simulation test results of the secondary control layer with different parameter settings for the gain K_C and the coefficient B_I. All horizontal scales are time in seconds. The BCDU Current plot shows the two BCDU output current responses in amperes, the BCDU Voltage plot shows the two BCDU output voltage responses in volts, the BCDU Power plot shows the two BCDU output power responses in watts, and the UCE plot shows the responses of each BCDU in volts.

Figure 10 and 11 show the dynamic response at different gains K_C. In both cases, the coefficient $B_I = 0.01\ \Omega$. Figure 10 shows $K_C = 1$, the critical value for system stability. The voltage and UCE responses shown in Figure 10 exhibit significant oscillation. A substantially improved dynamic response is found at $K_C = 0.3$. The voltage and UCE responses at this gain are shown in Figure 11.

Figure 12 and 13 show the dynamic responses at different B_I with a fixed control gain of $K_C = 0.3$. Figure 12 shows the dynamic responses of the battery discharging currents and power at $B_I = 0.1\ \Omega$. Compared to the dynamic responses at $B_I = 0.01\ \Omega$ as shown in Figure 10 and 11, a clear improvement is obtained at $B_I = 0.1\ \Omega$. Further increase of the coefficient to $B_I = 0.2\ \Omega$ results in the dynamic responses shown in Figure 13. These responses present some oscillation during transients. Based on the simulation test results shown in Figure 10 – 13, it is concluded that the best parameter setting for the simulation model in these tests are $K_C = 0.3$ and $B_I = 0.1\ \Omega$.

The effects of three-level hierarchical control are shown with the simulation test results presented in Figures 14-16. These simulation tests explore two constant loads ($P_{L1} = 1000$ Watts, $P_{L2} = 4500$ Watts) and different initial BES SoCs ($SoC_1 = 0.8, SoC_2 = 0.78$). In Figure 14-16, the Load Power plot shows the power of two loads in watts, the BCDU Voltage plot shows the two BCDU output voltage responses in volts, the BCDU Power plot shows the two BCDU output power responses in watts, and the SoC plot shows the responses of the two battery state-of-charges. All horizontal scales are time in seconds.

Figure 14 shows the simulation results when only the primary control (droop control) is used. In this case, the output voltages of both BCDUs are below 120 V while the voltage setting of the two BCDUs are 120 V. It shows that the load power sharing of the two batteries are different; one being 2000 W and another 3500 W. The difference between the two battery SoCs increases over time because of unbalanced load power sharing.

The waveforms shown in Figure 15 are the simulation results when both the primary control and secondary control are used. The bus voltage setting is 120 V. The figure confirms that the average BCDU output voltage is 120 V. The two batteries share load power equally (2750 W). The difference between the two battery SoCs keeps constant over time because of the balanced load power sharing.

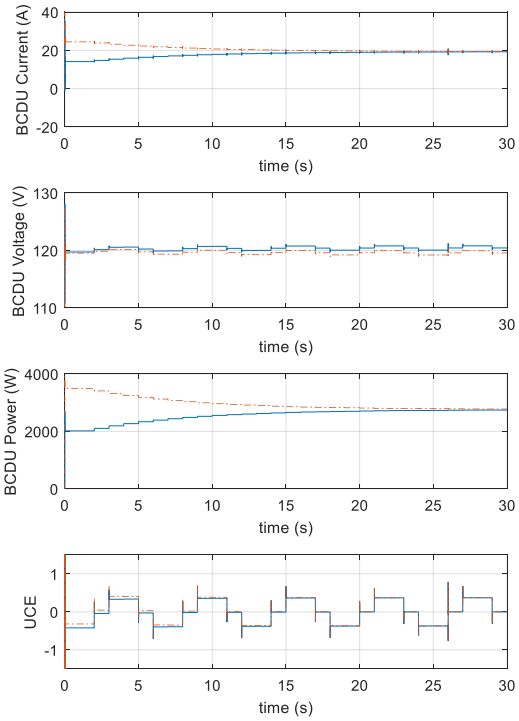

Fig. 10. Simulation results with K_C = 1, B_I = 0.01

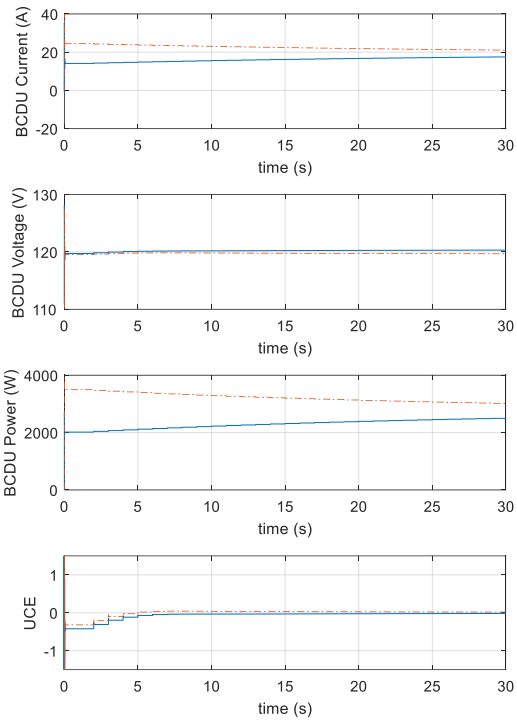

Fig. 11. Simulation results with K_C = 0.3, B_I = 0.01

The waveforms shown in Figure 16 are the simulation results with the three-level hierarchical control approach proposed in this work. The bus voltage setting is 120 V. The figure shows that the average BCDU output voltage is 120 V although the difference of two battery output voltages was greater at the beginning of the simulation when the tertiary control scheduled different load sharing weights for the different battery SoCs. Because of the different battery SoCs, the tertiary controller schedules load sharing weights which drive the two battery SoCs to equalize as soon as possible. At the beginning phase, BU-1 discharged at its maximum output current 31.25 A and shared load power of about 4469 W while BU-2 shared the rest of the load power, about 1031 W. The difference between battery load power output began reducing when the SoC difference became small enough. The system reached balanced load sharing when the battery SoCs became balanced. The figure shows the complete procedure of the two battery SoCs reaching and staying balanced during a 15 minute battery discharging operation.

To study more general operation with the proposed hierarchical control approach, a simulation test is performed with a fixed load of 1864 W and the variable load between 1000 W to 4200 W. The initial SoCs of BU-1 and BU-2 are 0.8 and 0.75, respectively. Figure 17 shows the waveforms of these simulation results.

VII. Conclusions

A novel hierarchical control approach is developed for the battery discharge management of a DCMG designed for a notional Gateway EPS. The UCE definition substantially simplifies the design of the centralized controller at the secondary control level and is effective at restoring the average voltage of the DCMG and in implementing accurate battery current sharing. Current sharing of distributed BUs is determined by the weights included in the UCE definition. These weights are evaluated at the tertiary control level based on battery SoCs with the purpose to implement SoC balancing discharge or restore equal SoCs of the distributed batteries in the DCMG. System digital simulation tests were performed with the same simulation model used in the NASA AMPS Modular Hardware Emulator and the proposed hierarchical control approach. The simulation results confirmed the effectiveness of the approach.

VIII. Acknowledgments

The work is supported by NASA faculty fellowship program 2019.

Identify applicable funding agency here. If none, delete this text box.

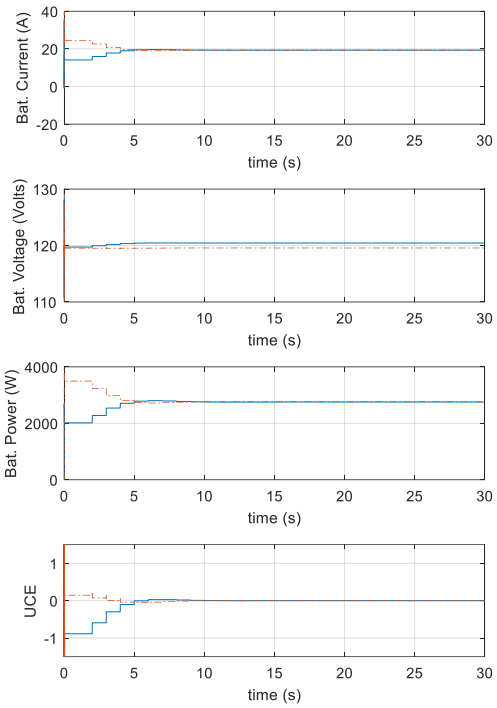

Fig. 12. Simulation results with K_C = 0.3, B_I = 0.1

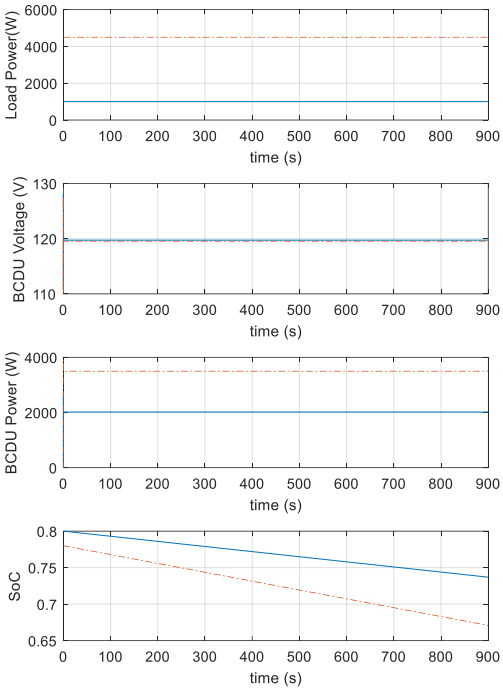

Fig. 14. Simulation results without secondary control

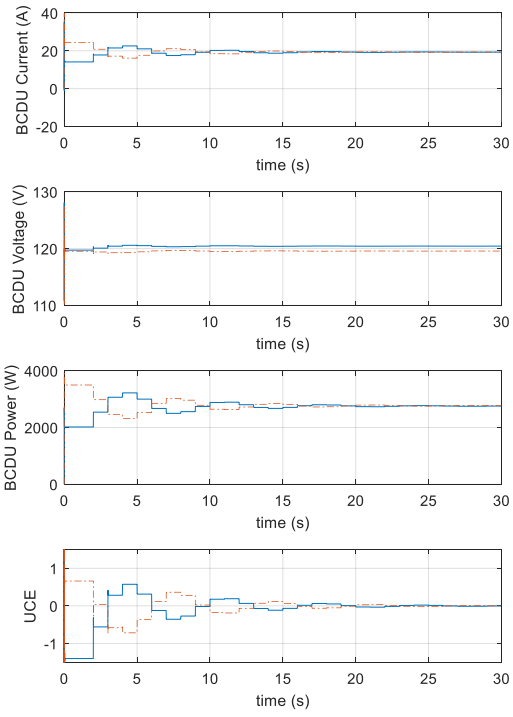

Fig. 13. Simulation results with K_C = 0.3, B_I = 0.2

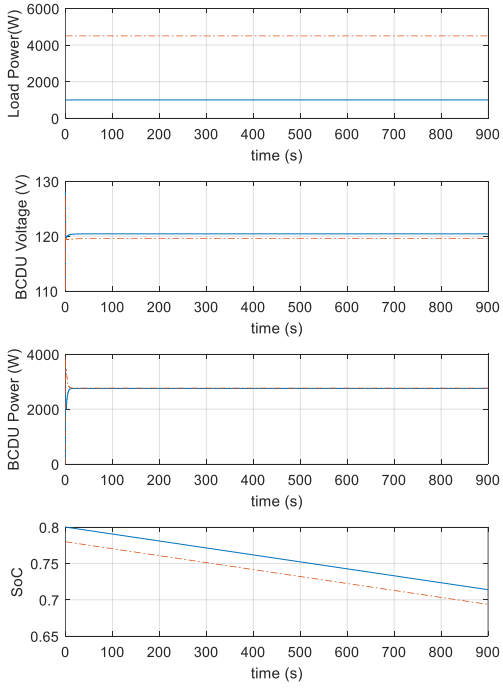

Fig. 15. Simulation results with secondary control

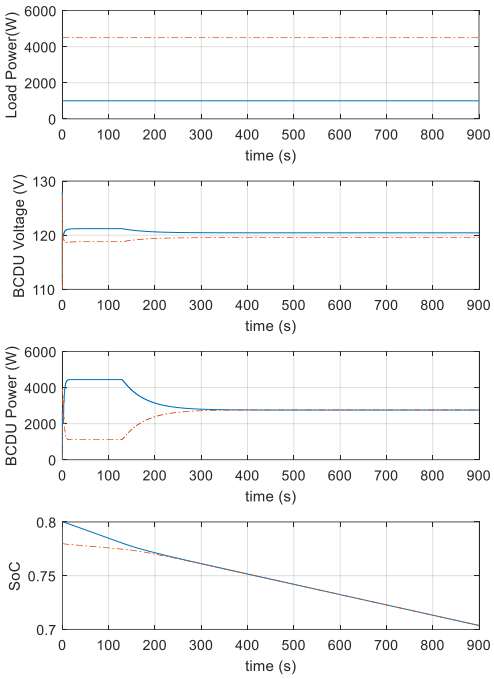

Fig. 16. Simulation results with secondary and tertiary control

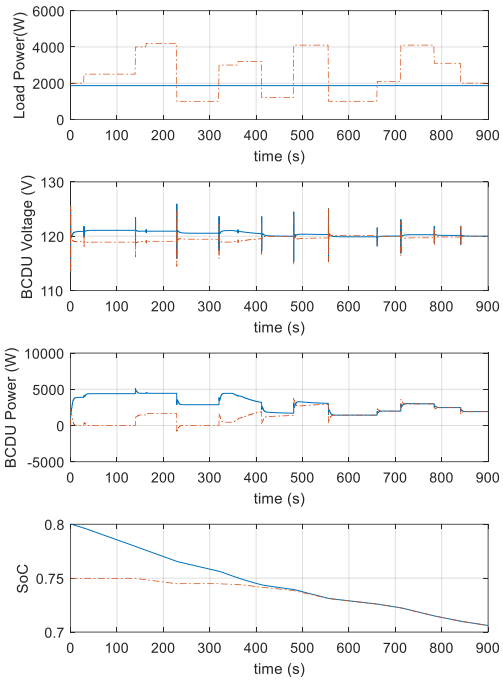

Fig. 17. Simulation results with secondary and tertiary control with fixed load of 1865W and variable load of 1000-4200 W

References

[1] J, Duncan Glover, M. S. Sarma, T. J. Overbye, "Power System Analysis and Design," 6th ed., Cengage Learning, ISBN-10: 1305632133, ISBN-13: 978-1305632134

[2] https://www.nasa.gov/johnson/exploration/gateway

[3] H. Hoang and S. J. Fu, "International Space Station Power System Requirements Models and Simulation," 2012 IEEE Aerospace Conference

[4] H. O. Aintablian and S. Wang, and S. D. Silva, "Simulation and analysis of the International Space Station US Laboratory electric power system," 35th Intersociety Energy Conversion Engineering Conference and Exhibit (IECEC) (Cat. No.00CH37022)

[5] Zhi Qiao and Jin Yang, "Comparison of centralized and distributed battery energy storage systems in LV distribution networks on operational optimisation and financial benefits," The Journal of Engineering, Vol. 2017, Issue 13, pp. 1671-1675

[6] Shubh Lakshmi and Sanjib Ganguly, "Centralized and Distributed Battery Energy Storage System for Peak Load Demand Support of Radial Distribution Networks," Proceedings of 2019 IEEE Milan PowerTech, June 23-27 2019 Milan, Italy.

[7] A. M. McNelis, R. F. Beach, J. F. Soeder, N. B. McNelis, R. May, T. P. Dever, and L. Trase, "Simulation and Control Lab Development for Power and Energy Management for NASA Manned Deep Space Missions," Propulsion and Energy Forum, July 28-30, 2014, Cleveland, OH

[8] J. Soeder, P. Raitano, and A. McNelis, "Intelligent (Autonomous) Power Controller Development for Human Deep Space Exploration," Presentation to Space Power Workshop 2016, Los Angeles, California, April 20, 2016

[9] J. Csank, J. Soeder, J. Follo, M. Muscatello, M. Carbone, and Y. H. Hau, "Autonomous Power Controller For the NASA Human Deep Space Gateway," 2018 International Energy Conversion Engineering Conference, July 10, 2018, Cincinnati, OH

[10] T. Dragicevic, P. Wheeler, and F. Blaabjerg, "DC Distribution Systems and Microgrids," The Institution of Engineering and Technology, ISBN-10: 1785613820, ISBN-13: 978-1785613821

[11] T. L. Vandoorn, J. C. Vasquez, J. De Kooning, J. M. Guerrero, and L. Vandevelde, "Microgrids, Hierarchical Control and an Overview of the Control and Reserve Management Strategies," IEEE Industrial Electronics Magazine, vol. 7, no. 4, pp. 42-55, Dec. 2013

[12] L. Meng, Q. Shafiee, and etc. "Review on Control of DC Microgrids and Multiple Microgrid Clusters," IEEE Journal of Emerging and Selected Topics in Power Electronics, vol. 5, No. 3, Sept. 2017, pp. 928 – 948

[13] J. M. Guerrero, J. C. Vasquez, J. Matas, D. Vicuna, L. Garcia and M. Castilla, "Hierarchical control of droop-controlled AC and DC microgrids: A general approach toward standardization," IEEE Transactions on Industrial Electronics, vol. 58, no. 1, pp. 158-172,2011.

[14] J. M. Guerrero, M. Chandorkar, T.L. Lee, and P.C. Loh, "Advanced control architectures for intelligent microgrids, part I: decentralized and hierarchical control," IEEE Transactions on Industrial Electronics, vol. 60, no. 4, pp. 1254-1262, 2013.

[15] M. Shahbazi, B. Kazemtabrizi, and C. Dent, "Coordinated Control of DC Voltage Magnitudes and State of Charges in Cluster of DC Microgrids," Proceedings of 2016 IEEE PES Innovative Smart Grid Technologies Conference Europe (ISGT-Europe).

[16] H. Wen, K. Zheng], and Y. Du, "Hierarchical Coordinated Control for DC Microgrid with Crowbar and Load Shedding Control," 2017 IEEE 3rd International Future Energy Electronics Conference and ECCE Asia, pp. 2208 – 2212

[17] Y. Han, X. Ning, P. Yang, and L. Xu, "Review of Power Sharing, Voltage Restoration and Stabilization Techniques in Hierarchical Controlled DC Microgrids," IEEE Access Vol. 7, 2019, pp. 149202 – 149223

[18] D.-H. Dam and H.-H. Lee, "A power distributed control method for proportional load power sharing and bus voltage restoration in a DC microgrid," IEEE Trans. Ind. Appl., vol. 54, no. 4, pp. 3616 - 3625, Aug. 2018.

[19] S. Peyghami, P. Davari, H. Mokhtari, P. C. Loh, and F. Blaabjerg, "Synchronverter-Enabled DC Power Sharing Approach for LVDC Microgrids," IEEE Trans. Power Electron., 2017, 32, pp. 8089 – 8099

[20] A. Vuorinen, "Planning of Optimal Power System," Publisher: Ekoenergo Oy, Jan. 1, 2007

[21] K. D. Hoang and H. Lee, "Accurate Power Sharing With Balanced Battery State of Charge in Distributed DC Microgrid," IEEE TRANSACTIONS ON INDUSTRIAL ELECTRONICS, VOL. 66, NO. 3, MARCH 2019

[22] J. X. Han, and W. Xiao, "Advanced Control Scheme for DC Microgrid via Dual Active Bridge and Bus Signaling," 2019 IEEE pp. 2515-2520

[23] H. Cai and G. Hu, "State-of-Charge Balancing of Grid-Connected Battery Energy Storage System," IEEE TRANSACTIONS ON INDUSTRIAL INFORMATICS, VOL. 12, NO. 5, OCTOBER 2016, pp. 1919-1929

[24] T. L. Vandoorn, J. C. Vasquez, J. D. Kooning, J. M. Guerrero, and L. Vandevelde, "Microgrids Hierarchical Control and an Overview of the Control and Reserve Management Strategies," IEEE industrial electronics magazine, December 2013, pp. 42-55

[25] C. Jin, P. Wang, J. Xiao, Y. Tang, and F. H. Choo, "Implementation of Hierarchical Control in DC Microgrids," IEEE TRANSACTIONS ON INDUSTRIAL ELECTRONICS, VOL. 61, NO. 8, AUGUST 2014, pp. 4032-4042

[26] S. Anand, B. G. Fernandes, J. M. Guerrero, "Distributed control to ensure proportional load sharing and improve voltage regulation in lowvoltage dc microgrids," IEEE TRANSACTIONS ON POWER ELECTRONICS, VOL. 28, NO. 4, APRIL 2013

[27] V. Nasirian, A. Davoudi, F. L. Lewis, and J. M. Guerrero, "Distributed Adaptive Droop Control for DC Distribution Systems," IEEE TRANSACTIONS ON ENERGY CONVERSION, VOL. 29, NO. 4, DECEMBER 2014, pp. 944 – 956

[28] X. Lu, J. M. Guerrero, K. Sun, and J. C. Vasquez, "An Improved Droop Control Method for DC Microgrids Based on Low Bandwidth Communication With DC Bus Voltage Restoration and Enhanced Current Sharing Accuracy," IEEE TRANSACTIONS ON POWER ELECTRONICS, VOL. 29, NO. 4, APRIL 2014, pp. 1800-1812

[29] P. Wang, X. Lu, X. Yang, W. Wang, and D. Xu, "An Improved Distributed Secondary Control Method for DC Microgrids With Enhanced Dynamic Current Sharing Performance," IEEE TRANSACTIONS ON POWER ELECTRONICS, VOL. 31, NO. 9, SEPTEMBER 2016, pp. 6658-6673

[30] T. R. Oliveira, W. W. A. G. Silva, and P. F. Donoso-Garcia, "Distributed Secondary Level Control for Energy Storage Management in DC Microgrids," IEEE TRANSACTIONS ON SMART GRID, VOL. 8, NO. 6, NOVEMBER 2017, pp. 2597-2607

[31] L. Meng, T. Dragicevic, J. Vasquez, J. Guerrero, and E. R. Sanseverino, "Hierarchical Control with Virtual Resistance Optimization for Efficiency Enhancement and State-of-Charge Balancing in DC Microgrids," in Proc. IEEE 1st Int. Conf. DC Microgrids (ICDCM), Jun. 2015, pp. 1–6.

[32] A. Kasis, E. Devane, C. Spanias, and I. Lestas, "Primary frequency regulation with load-side participation Part I: stability and optimality," IEEE Transactions on Power Systems, 2017, Vol. 32, Issue 5, pp. 3505-3518

[33] H. Cai, and G. Hu, "Distributed Control Scheme for Package-Level State-of-Charge Balancing of Grid-Connected Battery Energy Storage System," IEEE TRANSACTIONS ON INDUSTRIAL INFORMATICS, VOL. 12, NO. 5, OCTOBER 2016, pp. 1919-1929